Designing a High-Sensitivity Dual-Band Nano-Biosensor Based on Petahertz MTMs to Provide a Perfect Absorber for Early-Stage Nonmelanoma Skin Cancer Diagnostic

Musa N. Hamza, Mohammad Tariqul Islam, *Senior Member, IEEE*, Sunil Lavadiya, *Member, IEEE*, Slawomir Koziel, *Fellow, IEEE*, Iftikhar ud Din, and Bruno Cavalcante de Souza Sanches, *Member, IEEE*

***Abstract*—The purpose of this study is the development of a novel high-performance low-petahertz (PHz) biosensor for nonmelanoma skin cancer (NMSC) diagnosis. The presented device is designed to work within a microwave imaging (MWI) regime, which is a promising alternative to conventional diagnostic methods such as visual examination, dermoscopy, and biopsy. The suggested biosensor incorporates a dual-band perfect absorber (operating bands at 0.909 and 1.215 PHz) constructed using aluminum layers separated by a dielectric material. Numerical studies confirm its suitability for NMSC diagnosis, enabling discrimination between healthy and cancerous skin tissues and precise visualization of affected areas. Compared to existing THz devices, the proposed biosensor offers improved sensitivity, a smaller size, and enhanced resolution, attributed partially to the transition to the PHz band. Moreover, our research highlights the potential of PHz spectroscopy for biomarker detection, advancing noninvasive MWI techniques for NMSC and other skin cancers. The proposed biosensor boasts higher sensitivity, figure of merit (FOM), and quality factor (Q-factor), while its insensitivity to polarization angle ensures superior signal-to-noise ratio and high-resolution imaging, instilling confidence in specialists.**

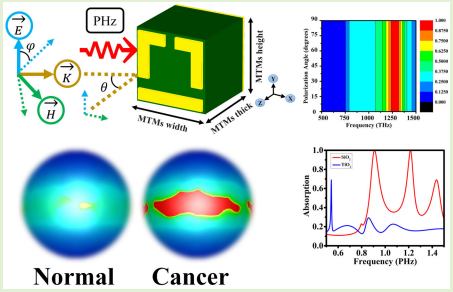

***Index Terms*— Biosensors, cancer detection, metamaterials (MMTs), perfect absorber, skin cancer.**

I. Introduction

BASAL cell carcinoma (BCC) results from the uncontrolled proliferation of basal cells due to DNA damage [1]. Skin cancer, including nonmelanoma skin cancer (NMSC), is widely diagnosed in the United States and is estimated to affect one in five Americans [2], [3]. Globally, skin cancer rates are increasing, with NMSC being the most common type, often growing slowly and locally [2], [4]. Although the risk of metastasis is low, NMSC can cause significant morbidity and disfigurement [5]. BCC accounts for 75% of NMSC cases, presenting as shiny papules or ulcers that do not heal. Cutaneous squamous cell carcinoma (cSCC), another type of NMSC, appears as erythematous patches or plaques. Early detection of cSCC speeds recovery and reduces treatment costs. Problems in diagnosing BCC arise from the subcutaneous localization of basal cells, which prevents early recognition [4], [6], [7]. This information highlights the need to improve early detection methods to minimize the impact of NMSC on health systems and public health worldwide. Researchers are currently engaged in intensive investigation of the refractive index (RI) sensor, considering it a dependable method yielding conclusive outcomes. RI sensing is crucial for real-time biosensing, aiding in applications like medical diagnosis. RI measurements offer insights into parameters like concentration, density,

Manuscript received 2 April 2024; accepted 10 April 2024. Date of publication 26 April 2024; date of current version 31 May 2024. This research was funded by the Ministry of Higher Education (MOHE), Malaysia through the Fundamental Research Grant Schemes (FRGS) under the grant number FRGS/1/2021/TK0/UKM/01/6 and the part of this research is supported by the Icelandic Research Fund Grant 239858 and by National Science Centre of Poland Grant 2020/37/B/ST7/01448. The associate editor coordinating the review of this article and approving it for publication was Dr. Ponnalagu R. N. *(Corresponding authors: Musa N. Hamza; Mohammad Tariqul Islam.)*

Please see the Acknowledgment section of this article for the author affiliations.

Digital Object Identifier 10.1109/JSEN.2024.3391347

and stress, crucial for identifying substances. In medical diagnostics, RI sensing is increasingly used to detect cancerous tumors by monitoring biomarkers like circulating tumor cells, highlighting its importance in early cancer detection and monitoring [8], [9], [10], [11].

Perfect absorbers offer enhanced sensitivity for RI sensing due to near-unity absorption, enabling the detection of subtle changes without labeling agents and operating across a wide range of refractive indices. They are versatile across frequencies, broadening their applicability. Researchers explore absorber models rooted in quantum mechanics for petahertz (PHz) applications, albeit with complex geometries [12], [13]. Innovations in design methods and components are pursued to enhance absorber quality, aiming for efficiency and broadband capability with angular and polarization insensitivity [14]. Numerous proposals have surfaced for the conceptualization of biosensors spanning from the gigahertz to the terahertz (THz) range, and extending into higher frequency domains like the PHz. Metamaterials (MMTs) have assumed a distinctive function in realizing targeted resonance frequencies within these spectrums, particularly within biomedical contexts, notably for the early identification of diverse forms of cancer [15], [16], [17]. THz metasurfaces leverage high-Q Electromagnetically Induced Transparency (EIT) resonances, achieving 0.55 THz/RIU sensitivity. Bright-dark mode coupling at 1.96 THz enhances sensitivity, with 0.04 THz (BCC versus healthy) and 0.02 THz (increasing BCC density) frequency shifts suggesting quick cancer screening [18]. A plasmonic-based sensor achieves 99.22% absorption and 24 680 nm/RIU RI sensitivity for breast cancer detection [19]. For colon cancer, a noninvasive diagnostic method using InSb identifies spectrum changes in response to THz pulses, distinguishing healthy from malignant tissue [20]. A THz biosensor with perfect MMT absorption enables basal cell cancer diagnosis, with frequencies at 0.78 and 0.904 THz [8]. Laser-induced fluorescence (LIF) and diffuse optical spectroscopy (DOS) show promise for skin cancer diagnosis, demonstrating high sensitivity and specificity [21]. A dual-band plasmonic metasurface detects hemoglobin concentrations, suggesting advancements in medical diagnostics [22]. MMTs allow tailored responses to specific wavelengths [23], offering heightened sensitivity to minute changes associated with early-stage cancerous tissue. They also enable high resolution and specificity, facilitating early intervention. Challenges like technology development and clinical validation persist, underscoring the need for ongoing research to realize their potential for improved patient outcomes. MMTs offer potential for sleeker and more effective metamaterial absorbers (MMAs) in nano-sized structures [23]. MMTs' unique behavior, characterized by negative permittivity, permeability, and RI [24], enhances MMA performance by absorbing most electromagnetic (EM) wave radiation. Additionally, MMT nano-resonators enable the excitation of surface plasmonic resonance (PSPR, LSPR), further enhancing absorber efficiency through interaction with incident waves [25]. Nano-biosensing systems enable health monitoring and disease detection. Advancements in sensor miniaturization shift communication from low-frequency (microwaves) to high-frequency (THz and beyond) EM waves, prompting the study of radiation effects on human tissues [26], [27], [28]. In MMA research, advancements have enabled designs covering larger frequency ranges, including infrared and visible frequencies. Typically employing a metal-insulator-metal (MIM) configuration, these absorbers utilize a resonator on the top metal layer to eliminate EM radiation at the ground metal layer while employing a dielectric layer for coupling capacitance. Effective impedance matching between the MMT surface and free space minimizes wave reflection back into space [29], [30], [31].

MMAs utilizing metals like gold or silver offer increased absorption rates due to the plasmonic effect, but their high cost necessitates alternatives. Aluminum (Al) has emerged as a cost-effective substitute without compromising performance. To address this, a tri-layer MMA composed of Al-Silicon dioxide-Al, with a total thickness of 110 nm, is proposed. This design aims to achieve simplicity and efficacy in the PHz spectrum.

The potential application of the 0.5 to 1.5 PHz frequency range for medicine, especially in the diagnosis of NMSC, represents an emerging area of research development.

EM waves at low PHz frequency bands interact with tissues primarily through absorption, scattering, and reflection phenomena. At these frequencies, waves may be absorbed by biological tissues, where the extent of absorption depends on the tissue's dielectric properties, which include factors such as the complex RI, conductivity, and water content [28], [29], [30], [31], [32].

PHz waves can also undergo scattering when encountering structures within tissues, probably when they have dimensions comparable to the wavelength of the radiation. Cellular structures, organelles, and macromolecules within tissues could scatter PHz waves. The scattering behavior may provide information about tissue microstructure and organization, which could be exploited for sensing purposes [26].

PHz waves in this frequency range exhibit unique interactions with biomolecules and functional groups, potentially increasing sensitivity and specificity for detecting subtle changes associated with NMSCs [32], [33], [34]. Additionally, this range may provide improved spatial resolution compared to lower frequencies, facilitate visualization of finer features in skin lesions, and potentially enable label-free detection [33], thereby simplifying the process and reducing the risks associated with screening agents. However, challenges such as the immaturity of the technology, limited research, and the need for a deeper biological understanding of PHz wave interactions with healthy and cancerous skin tissues hinder widespread clinical use. Currently, the diagnosis of NMSC relies primarily on visual examination, dermoscopy, and biopsy, with PHz technology in the 0.5–1.5 PHz range not yet integrated into clinical practice. However, ongoing research shows promise for earlier and more accurate detection of CNMS, noninvasive diagnosis, and improved differentiation between benign and malignant lesions, emphasizing the importance of continued exploration to fully realize the potential for improving CNMS diagnostics in the future.

Below are some of the studies designed using PHz MMTs and nanoscale MMTs for different applications. The bulk of suggested MMAs are best designed using multilayer structures, namely MIM [35], especially for the PHz range. An MIM structure (Ni–SiO_2–Ni) MMA with a mean absorption of 95.77% and a peak absorption of 99.999% at 772.82 nm was demonstrated by Shuvo et al. [36]. It also shows excellent wideband absorption between 300 and 1600 nm. An MXene-based fractal MMT solar absorber for use in the visible and near-infrared wavelengths is described in work in [37]. An MXene fractal pattern sheet supported on a SiO_2 substrate and a silver reflecting surface forms this absorber, which exhibited strong absorption—above 85% for visible and near-infrared bands. A nanoscale absorber with an average absorption of 93% over a wide optical window of 400 to 2800 nm has been published by Bilal et al. [31]. Two 500 nm-period MMAs were constructed in [38] for comparative reasons. These MMAs demonstrated strong adaptability for absorption rates exceeding 88% when examined for two distinct forms. An aluminum (Al)-based structure and titanium-silica (Ti-SiO_2) cubes were used in a method described by Lei et al. [39] to achieve nearly perfect absorption. The structure shows an average absorbance of 97% over a broad range of wavelengths, from visible to near-infrared (354 to 1066 nm), with a 90% absorption bandwidth spanning 712 nm and an absorption peak exceeding 99.8%. The study [40] reported on a hexagonal ring resonator-based MMA with a small unit cell size of 66×66 nm^2. This absorber offered an operating range of 380–2500 nm and a maximum absorption of 99% with an angular stability of up to 70°. These characteristics made this absorber a useful media for a range of uses. An MMA with an absorbance of more than 90% covering 380 to 2500 nm and a mean absorbance of 96.64% throughout the functional bandwidth, with a 99% absorption peak visible at 618 nm, was proposed by Hakim et al. [41]. Utilizing its absorption properties, a MMA created in [42] harvests energy in the visible spectrum. A stepped impedance resonator, which makes up the unit cell of the MMA, has dimensions of 500 nm on each side. This feature enables the MMA to have an absorption rate exceeding 90% throughout the visible spectrum. Mahmud et al. [43] presented a design in this work that produced an average absorption of 96.77% between 389.34 and 697.19 nm and a 99.99% absorption at 545.73 nm for TEM mode. The design also achieved over 97% absorption with a bandwidth of 102 nm.

This study introduces a new ultrawideband nanostructured MMA featuring an Octagon-Packed Star-Shaped resonator designed for the range of UV (200–400 nm) to NIR (700–900 nm) wavelengths. By design and analysis, the absorber exhibits outstanding performance, displaying effective absorption levels throughout the specified wavelength ranges. This advancement shows potential for applications in UV to NIR sensing, imaging, and energy harvesting technologies [44]. This article describes a MIM MMA that is insensitive to polarization and exhibits nearly complete absorption across a broad spectrum (300–1600 nm). It maintains an average absorption rate of 95.77% and reaches a peak of 99.999% at 772.82 nm. The absorber shows stability when subjected to wide incident angles and mechanical bending. Its suitability for solar cell use is validated under Air Mass (AM) 1.5 solar spectrum conditions, indicating potential for various optical applications beyond [36]. The study presents a straightforward efficient nanostructured absorber made up of a circular nickel ring, which provides high-bandwidth absorption (93%) ranging from 400 to 2800 nm. It exhibits insensitivity to polarization, stability against changes in angle, and cost-effectiveness. This absorber sustains an average absorption of 80% at oblique angles, showing promise for energy harvesting and thermal applications [31]. This study introduces a MMA that is not affected by oblique angles or polarization. It is created using tungsten resonators on a silicon dioxide base, enhanced with SiO_2 coatings. This MA records a remarkable 92% average absorption rate between 400 and 2400 nm, remaining stable at oblique angles up to 45°, and it is indifferent with polarization. Its compatibility with solar absorption and optical filters makes it a versatile choice for various optical applications [45]. The study introduces an ultrabroadband absorber constructed from tungsten, aluminum trioxide, and titanium nano disks arranged elliptically. It achieves 94% average absorptivity across the 500 to 1800 nm range, with complete absorption at 1200 nm. The absorber exhibits polarization insensitivity and wide-angle characteristics, owing to surface plasmon resonances, making it applicable in solar absorbers, photodetectors, and other fields [46]. The study presents a planar square meta-ring absorber comprising nickel and aluminum nitride dielectric, offering wideband absorption from 400 to 3000 nm. With average absorption exceeding 90% and maintaining 70% for oblique angles, it shows polarization insensitivity due to its geometric symmetry, indicating potential for energy harvesting and optoelectronic applications [47]. The research introduces two ultrabroadband MMAs utilizing anti-reflection coatings of SiO_2 and Si_3N_4, along with a Ti-SiO_2-Ti metasurface. These coatings notably enhance absorption bandwidth by 594 and 1093 nm, respectively. Both absorbers demonstrate high average absorptions (>95% and >87%), resilience to large incident angles, and potential uses in solar energy harvesting, thermal emitters, and photodetectors [48]. The article presents a fourfold star petal–shaped nanostructure functioning as a broadband plasmonic MMAs, working within the frequency range of 390 to 750 THz. It achieves a median absorbance exceeding 96% irrespective of polarization angles. Utilizing ultrathin chromium layers and SiO_2 dielectric, it shows promise for applications in energy harvesting, stealth technology, and biomedical sensors [49]. The research presents a hybrid MMA comprising multilayered cermet thin films with a tapered structure. By integrating optical interference and nano-cone structures, it attains a mean absorbance of over 98% across a broad spectrum (300–3000 nm) while maintaining good angular tolerance. Manufactured using colloidal lithography and magnetron sputtering on a flexible polyimide substrate, it demonstrates durability against bending and heating, suggesting potential for real-world applications [50]. This article introduces a Ni-PI-Ni based wideband MMA for visible

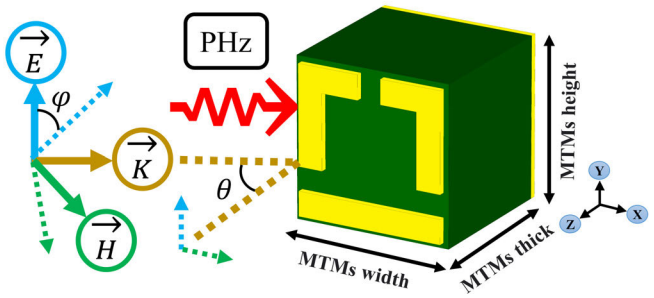

Fig. 1. Structural design and incident field directions of a perfect absorber.

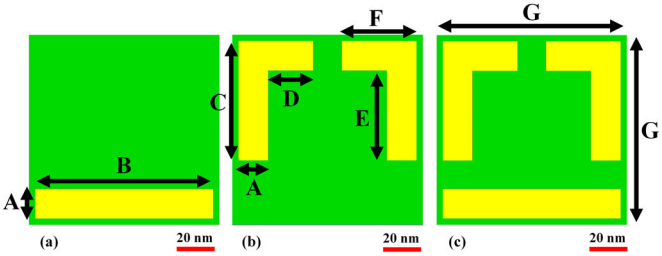

Fig. 2. Recommended structural design for a perfect absorber: (a) model 1, (b) left and right of the model 2, and (c) model 4 (proposed biosensor design).

and near-infrared applications. With a compact unit cell size, it achieves 98.16% absorption from 380 to 2300 nm and 99% absorption over 685 nm [51].

II. Model's Unit Cell Layout

MMTs effectively absorb EM radiation due to their structural properties. THz waves interact with MMTs, resulting in transmission, reflection, and absorption, as seen in Fig. 1. Perfect absorbers strive to reduce reflection by absorbing most incident energy, whereas reflected waves bounce back off the MMT surface. The MMT's architecture reduces destructive interference and improves absorption. The MMA energy from transmitted waves to minimize transmission. The MMT structure attenuates or absorbs waves, providing control over transmission properties. Perfect absorbers aim to decrease transmitted energy. The design must consider the biosensor's sensitivity, specificity, and selectivity. These characteristics are crucial in determining the accurate diagnosis of skin cancer. Building biosensors for this application requires higher sensitivity and specificity, which might be challenging. Optimizing biosensor performance is critical for increasing clinical value and providing informative data for skin cancer diagnosis.

The proposed MMT-based absorber is shown in Fig. 2(c). The final model was created based on the combination of Model 1 and Model 2, as shown in Fig. 2(a) and (b). The dual-band response is achieved based on the combination of these two models. The suggested design has perfect conducting layers in the bottom and top regions. The dielectric material is located between both conducting layers. Combining the models aims to avoid interacting magnetic and electrical forces, and overlapping. Table I provides a summary of the directional data from each model.

The suggested absorber was constructed with a commercial full-wave finite integration (FIT) approach based on a high-frequency EM solver for microwave studio. MMTs may be analyzed using numerical computations to identify their properties and how they function across various frequency ranges and boundaries. Scientists have used numerical analysis to analyze various structures such as perfect electric and magnetic conductors (PEC and PMC), unit cells, periodic arrays, and free space.

TABLE I
Complete List of the Variables That Have Been Adjusted for the Recommended Sensor

Parameter	Value (nm)	Parameter	Value (nm)
A	15.55	G	100
B	93.34	BBC Thick	100
C	62.8	BBC width	100
D	23.6	MTMs Thick	100
E	47.23	MTMs width	100
F	39.2		

To streamline simulation methods, a unit cell, was assigned in the x and y dimensions and an open add-space in the z-direction. The model's three-layered construction consists of Silver-metal at the top and bottom and a dielectric spacer composed of Silicon dioxide (SiO_2) in the center. Silver has a conductivity of 6.3012 10^7 S/m. Silicon dioxide (SiO_2) plays a critical role as a substrate material in MMAs, as in [31] and [45]. SiO_2 boasts high transparency across a broad spectrum, particularly in the visible and near-infrared ranges, minimizing interference with incident light and facilitating efficient interaction with desired wavelengths. Its low RI helps mitigate reflections at the substrate-MMT interface, reducing losses and optimizing absorption performance. Moreover, SiO_2's mechanical robustness and chemical inertness impart stability and durability to the MMA structure, ensuring long-term reliability even in challenging environmental conditions. Overall, SiO_2 serves as a versatile substrate material that enhances the optical performance, stability, and functionality of MMAs across various applications, ranging from the visible to near-infrared regions of the EM spectrum. The silver layers on the bottom and top were 4 nm thick. The top metal layer was designed to match the incident medium's impedance, allowing maximum power penetration and propagation in SiO_2. The bottom layer of silver blocks all EM waves and provides zero resistance for transmission-line theory (TLT) interpretation. Absorption systems with large electrical and/or magnetic losses catch moving waves, while a metallic layer at the bottom prohibits transmission. An EM wave impinged on the top plane was used to determine absorption parameters.

III. Results and Discussion

This section addresses the results of the proposed PHz biosensor in an incremental approach. First, the sensor will be evaluated part by part, constitutively iterating between its geometric components while analyzing its absorbance properties. The synthesis started with the determination of the block structure sizing and the tuning of the width of the bottom part of the device. Fig. 3(a) shows the absorbance curve for the selected structure, referenced as Model 1. Model 1 did not reach perfect absorption in any region of the evaluated

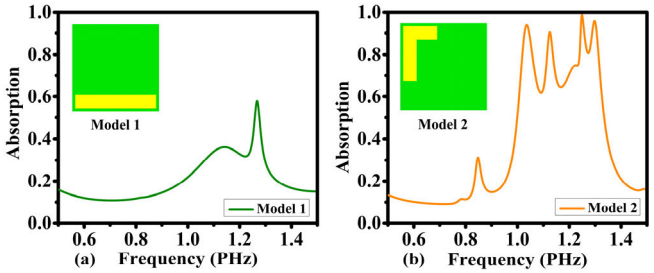

Fig. 3. These are the different absorption properties of the two designs: (a) Models 1 and (b) Model 2.

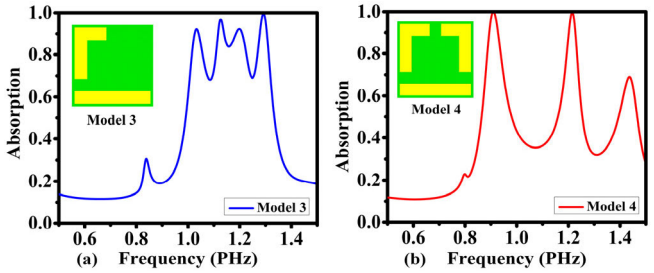

Fig. 4. These are the two designs' various absorption qualities: (a) Model 3 and (b) Model 4.

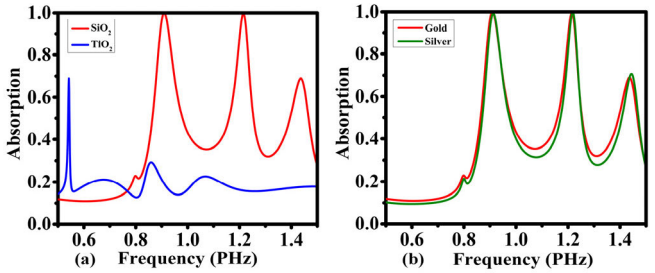

Fig. 5. Absorption spectra for the suggested design under various: (a) substrate material and (b) resonator material conditions.

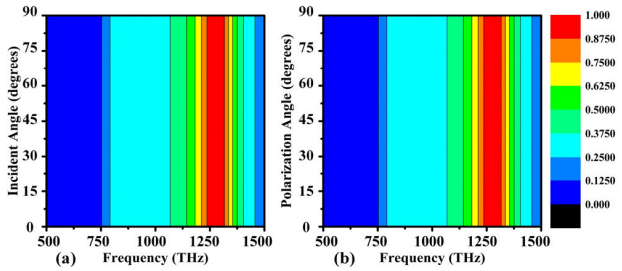

Fig. 6. Impact of angle modification on absorption rate is investigated for: (a) incidence angle and (b) polarization angle.

spectra, but it was already presenting a peak near 1.2 PHz, one of the regions of interest in this work. Fig. 3(b) shows the absorption spectra of Model 2, which addresses the L-shaped upper section. In this case, very high absorption was observed in the 1.25 PHz region and several smaller peaks also showed absorption of more than 0.8, the ones in 1.0, 1.1, and 1.3 PHz. The results are better than Model 1, but it still does not present good selectivity, and the values of the peaks are not maximized. Model 1 and Model 2 were then merged to create a mixed structure, which was labeled as Model 3. The absorption results of this model are presented in Fig. 4(a). Model 3 showed high absorbance peaks in 1.0, 1.1, 1.2, and 1.3 PHz, where the last was the only maximum. Its results were similar to Model 2, but it has some advantages, the peaks are more well-defined. It was observed that the absorber had important field interactions around the L shape and the bottom bar, and aiming to create a design with a dual-band profile, a new change to the structure was proposed. The L shape was duplicated and its distance was optimized to generate an absorbance peak, while the pair of L interacting with the bottom bar generates another peak. This design was named Model 4 and is shown in Fig. 4(b) together with its absorbance curve. Model 4 results presented very well-defined perfect absorbance peaks at 0.909 and 1.215 PHz, this was a very important improvement in relation to the previous models and with its dual-band characteristics, was adequate to the application in question and was selected as the proposed model in this work.

With the general geometry of the structure defined, an evaluation of the available constitutive materials was performed. Fig. 5 addresses the absorption profile of the sensor for distinct alternative substrate and conductor materials. For the substrate silicon dioxide and titanium dioxide were evaluated, and in this case, titanium dioxide performance was not adequate, making silicon dioxide a better alternative material as the substrate.

The selection of an optimal substrate material, such as silicon dioxide (SiO_2) or titanium dioxide (TiO_2), for the biosensor hinges on several key factors. At the operating frequencies (0.909 and 1.215 PHz), the material's permittivity and loss tangent are critical. A low-loss tangent is essential to minimize energy dissipation within the substrate. While both SiO_2 and TiO_2 are viable options in the PHz range, their properties may differ slightly, potentially influencing their interaction with the PHz waves. Additionally, fabrication compatibility with the chosen MMT design must be considered. While SiO_2 is well-established for nanofabrication, TiO_2, depending on its specific form (e.g., Rutile TiO_2), may offer additional functionalities. Finally, the substrate material can influence the overall sensitivity and specificity by affecting the interaction between the electric field and the target biomolecules.

The option of silicon is also very interesting as it may be integrated or reused for important work already done in the nanoelectronics area, where it is a very well-explored material. In the case of metallization, gold and silver had similar good results, presenting the same perfect absorbance peaks. This material can also be selected as it has appropriate integration in the fabrication process.

The design was then evaluated with respect to its response to changes in the incident angles of the wave and also for distinct polarizations. Fig. 6 presents the results of absorbance as a color map. The response of the proposed model for different incident angles is practically uniform and Fig. 6(a) shows that even with angles as high as 90° the structure still acts as a perfect absorber in the main desired band around 1.2 PHz. In the case of the response to polarization, it was observed in Fig. 6(b) that just very minor changes happened for this band and these facts were considerably important to the usage of the absorber as a sensor. Polarization and incident angle sensitivity can lead to distortion and poor imaging and detection quality and the proposed model behaved very well in this matter.

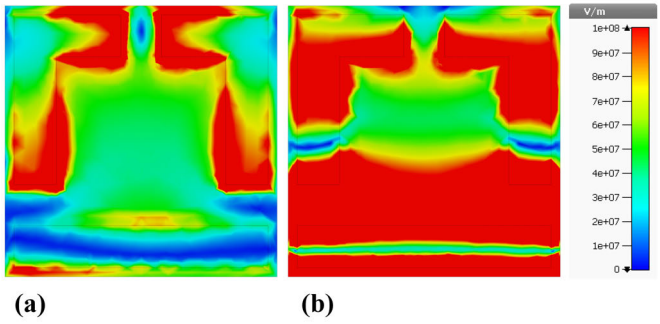

Fig. 7. Distributions of the MMT structure field are shown on a color map: (a) *E*-field at 0.909 PHz and (b) *E*-field at 1.215 PHz.

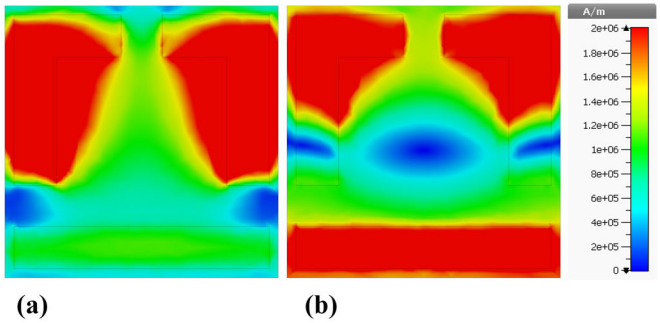

Fig. 8. Illustrated color map shows the field distributions of the proposed MMT structure: (a) *H*-field at 0.909 PHz and (b) *H*-field at 1.215 PHz.

Aiming to better analyze the EM internal working of the MMT, several field monitors were inserted into the design and plotted for the frequencies with greater relevance for this structure. Fig. 7(a) shows the electric field inside the structure for 0.909 PHz and Fig. 7(b) for 1.215 PHz. Fig. 7(a) contains the electric field plot for the lower band, where it is possible to see that this frequency range interacts strongly with the L-shaped structures on the top. On the other hand, Fig. 7(b) illustrates that the high absorption over 1.215 is linked to the interaction between the bottom bar and the top structures. For both cases in Fig. 7, the electric fields were considerable, but all were enclosed in the tolerable margins for the chosen materials. Here, the adequate electric field will provide a longer mean time between failures (MTBF) for the sensor. Finally, Figs. 8 and 9 provide the plots for the magnetic field and current distribution for the proposed sensor at 0.909 PHz and 1.215 PHz respectively. The surface current distributions results and the fields at Fig. 9(a) and (b) clearly agree with the conclusions made for the electric fields from Fig. 7, adding complementary information in respect to magnetic field strengths and about the internal behavior of the absorber. At a glance, the MMA works adequately in a dual-band approach achieving PHz frequency, and is qualified for the application, where the next section will address its application as a biosensor for NMSC.

IV. Diagnosis of NMSC

The NMSC diagnostic biosensor employs microwave imaging (MWI) to enhance early detection of cancer cells by accurately predicting and analyzing signal transmission and absorption. This innovative approach overcomes current barriers, potentially improving the diagnosis of NMSC. MWI offers

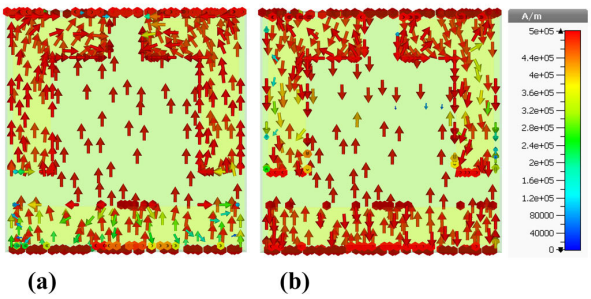

Fig. 9. Surface current distribution of the recommended MMT design: (a) at 0.909 PHz and (b) at 1.215 PHz.

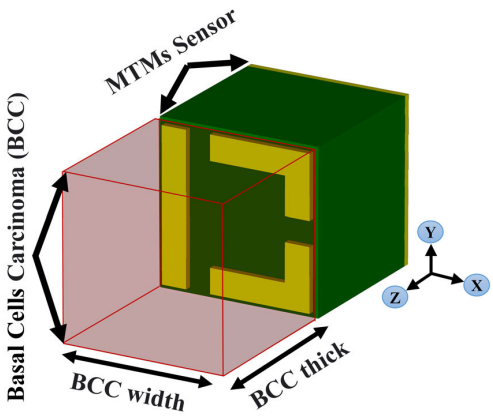

Fig. 10. Suggested biosensor investigates the absorption coefficient in both healthy skin and NMSC.

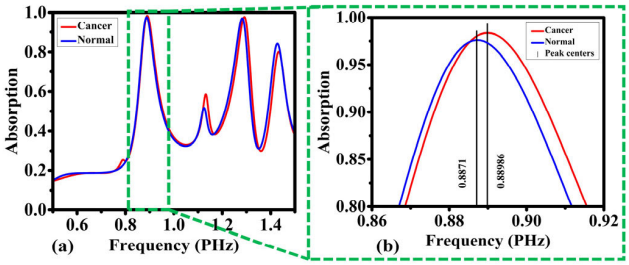

Fig. 11. Proposed biosensor detects the absorption coefficients for normal skin and NMSC; the frequency range is between: (a) 0.5–1.5 PHz and (b) 1.255–1.312 PHz.

a visually appealing tool that aids in identifying and diagnosing skin cancer in its early stages. The biosensor's ability to analyze MWI signals provides a reliable means of detecting abnormalities indicative of cancerous cells. Fig. 10 visually outlines the proposed sensor, demonstrating the biosensor's potential to revolutionize NMSC diagnosis through its advanced technology and precise analysis of microwave signals, ultimately enabling timely intervention and treatment for patients. To ensure accurate results, we sandwiched a skin sample between two coverslips, each with distinct refractive indices of 1.360 for healthy skin and 1.380 for NMSC [8], [52], [53], [54], [55], [56] as depicted in Fig. 10. This setup minimizes errors by providing a controlled environment for analysis. By utilizing coverslips with specific refractive indices, we optimize the detection process, enhancing the reliability of diagnosis based on variations in RI associated with different skin conditions [52], [53].

In Fig. 11(a), detection results are presented for healthy skin and NMSC. The analysis targeted the initial peak within

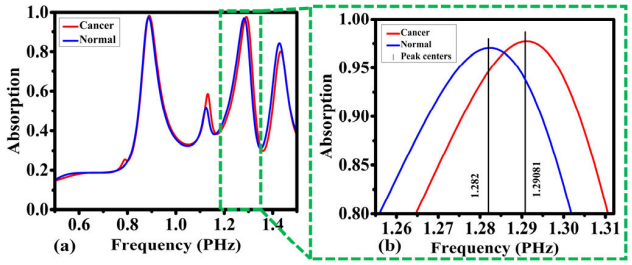

Fig. 12. Proposed biosensor evaluates the absorption coefficients for normal skin and NMSC; the frequency range is between: (a) 0.5–1.5 PHz and (b) 0.65–0.85 PHz.

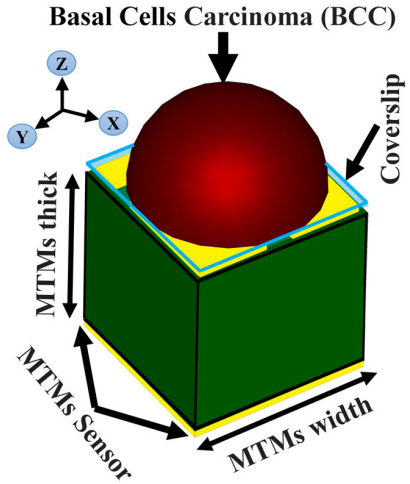

Fig. 13. Diagnosis of NMSC using the MWI approach.

the 0.5 to 1.5 PHz range for both skin conditions. Fig. 11(b) reveals a significant variation between healthy and cancerous skin samples, presenting a difference of 0.00276 PHz from 0.8871 to 0.88986 PHz. This difference underscores the potential of PHz imaging to discriminate subtle variations in skin composition, offering promise for enhanced diagnostic capabilities in distinguishing between healthy and cancer tissue with high precision and accuracy. In Fig. 12(a), the detection outcomes for healthy skin and NMSC are depicted. The investigation primarily concentrated on contrasting healthy and cancerous skin for the second peak, located within the 0.5 to 1.5 PHz range. As illustrated in Fig. 12(b), the findings exhibit a notable distinction between healthy skin and NMSC, with a visible difference of 0.00881 PHz ranging from 1.282 to 1.29081 PHz. This discrepancy emphasizes the potential of PHz imaging to effectively discriminate between healthy and cancer skin tissues, offering valuable insights for diagnostic and therapeutic interventions.

The study's outcomes were validated through MWI techniques, which rely on reconstructing images within the PHz frequency spectrum. This method employs principles allowing for detailed visualization. In Fig. 13, a section of skin was carefully positioned on a coverslip, serving as a substrate for analysis using the proposed biosensor. This approach offers a noninvasive means to examine biological samples, potentially providing valuable insights into their composition and properties. Such imaging methods hold promise for various applications in fields like medical diagnostics, materials

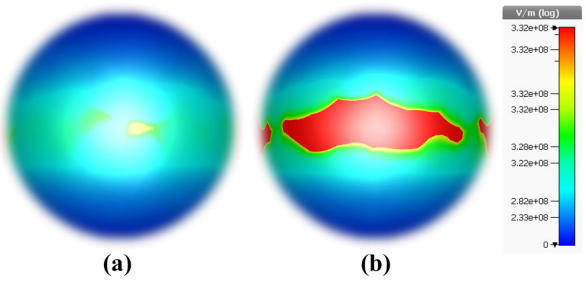

Fig. 14. MWI technique results: (a) healthy skin and (b) NMSC.

science, and beyond, owing to their ability to reveal details with high precision and accuracy. MWI, as depicted in Fig. 14, demonstrates a significant difference in electric field responses between normal and NMSC tissue.

The increased concentration of the electric field in cancerous areas is a phenomenon rooted in the distinct biophysical properties of cancerous tissues compared to their healthy counterparts. These differences manifest primarily in altered dielectric properties, cellular composition, and water content within the tissue microenvironment. Cancerous tissues often exhibit higher permittivity or conductivity, stemming from changes in cellular morphology, density, and composition associated with tumorigenesis and tumor progression. Consequently, the interaction between electric fields and cancerous tissues leads to localized enhancements of the electric field within cancerous regions. Furthermore, the abnormal morphology and distribution of cancerous cells contribute to variations in the tissue's electrical response, further accentuating the concentration of the electric field in cancerous areas. Additionally, the elevated water content in cancerous tissues, a characteristic feature of many tumors, influences the electric field distribution by virtue of water molecules' polar nature. This intricate interplay between tissue composition and EM field interactions underscores the complexity of cancer biophysics and highlights the importance of understanding these mechanisms for the development of advanced diagnostic technologies.

The increased concentration of the electric field in cancerous areas suggests MWI's ability to distinguish between healthy and malignant skin tissue based on electric field data. This ability is vital for early detection and treatment of skin cancer, allowing for noninvasive monitoring of tissue abnormalities. Additionally, MWI goes beyond diagnosis, aiding in controlling surgical procedures by accurately sketching tumor boundaries and assessing treatment effectiveness. Consequently, MWI presents itself as a versatile approach with substantial potential in both diagnosing and treating skin cancer.

V. Benchmarking

A comparative assessment was conducted to evaluate the efficacy of a newly proposed nano-biosensor operating in the PHz band for the early detection of NMSC. Utilizing MMT perfect absorber technology, the biosensor's performance was analyzed in terms of sensitivity, quality factor (Q-factor), and figure of merit (FOM), as depicted in Table II.

TABLE II
BIO-SENSING PERFORMANCE COMPARISONS OF VARIOUS SENSOR APPLICATIONS BASED ON MMT

Ref.	Q	S (THz/RIU)	FOM (RIU−1)	Bio-application	Year Published
[57]	5.58	0.02432	0.1216	detection of Penicillia	2014
[58]	-	0.0242, 0.02438	-	detection of Virus	2017
[59]	6.6	0.285	1.88	sensor	2020
[60]	-	0. 960	-	Biosensor, Collagen	2020
[61]	-	0. 2833	-	Polystyrene particle	2021
[62]	2.43	1.21	2.75	Cancer Diagnostics, Biosensor	2022
[63]	8.21, 6.05	0. 203	1.81, 1.57	sensor	2022
[64]	-	1.06	0.166	detection of avian influenza virus	2022
This work	7.81, 12.84	138, 440.5	1.186, 4.656	Non-Melanoma Skin Cancer Diagnostics	-

Significantly, the proposed nano-biosensor demonstrated substantial enhancements in sensitivity and overall performance compared to previous sensors, which were of micrometer size and operated in the THz range. Theoretically, the higher energy of PHz waves can lead to stronger interactions with specific biomolecules, potentially translating to a more sensitive biosensor capable of detecting subtle cancerous changes. Additionally, the shorter wavelengths of PHz waves offer the potential for superior spatial resolution, enabling more precise visualization of affected areas within the tissue sample. Furthermore, the possibility of unique spectral fingerprints for cancer markers in the PHz range, not readily observable in the THz regime, could lead to more specific detection. Notably, the transition to the PHz band offers improved resolution and specificity for detecting subtle changes associated with NMSC, while the nano-scale dimensions of the biosensor signify advancements in miniaturization. These findings underscore the potential of the MMT-based biosensor to revolutionize early cancer detection, offering superior performance and miniaturization for enhanced clinical applications.

VI. FUTURE PERSPECTIVE

Designing higher sensitivity biosensors for early cancer detection e.g., early-stage diagnosis of breast cancer, colon cancer, adrenal gland cancer (PC-12), cervical cancer (HeLa), and blood cancer using PHz EM wave imaging bio-sensors.

VII. CONCLUSION

In conclusion, this study presents a novel high-sensitivity dual-band nano-biosensor based on PHz MTMs for early-stage NMSC diagnosis. The biosensor integrates a dual-band perfect absorber, achieving enhanced sensitivity within the low PHz range (specifically, it exhibits operating bands at 0.909 and 1.215 PHz). Numerical simulations validate its efficacy in discriminating between healthy and cancerous tissues and facilitating precise visualization of affected areas. Comparative analysis against existing THz devices demonstrates improved sensitivity, smaller size, and superior resolution and specificity. Furthermore, the biosensor's insensitivity to polarization angle ensures superior signal-to-noise ratio and high-resolution imaging, instilling confidence in specialists. This research underscores the potential of MMT-based biosensors for early-stage cancer diagnosis, particularly highlighting the benefits of transitioning to higher frequency operating bands within the low PHz range, thus contributing to advancements in NMSC detection and treatment.

ACKNOWLEDGMENT

Musa N. Hamza is with the Department of Physics, College of Science, University of Raparin, Sulaymaniyah 46012, Iraq (e-mail: musa.nuraden@uor.edu.krd).

Mohammad Tariqul Islam is with the Department of Electrical, Electronic and Systems Engineering, Faculty of Engineering and Built Environment, Universiti Kebangsaan Malaysia (UKM), Bangi 43600, Malaysia (e-mail: tariqul@ukm.edu.my).

Sunil Lavadiya is with the Department of Information and Communication Technology, Marwadi University, Rajkot, Gujarat 360003, India (e-mail: sunil.lavadiya@marwadieducation.edu.in).

Slawomir Koziel is with the Engineering Optimization and Modeling Center, Reykjavik University, 102 Reykjavik, Iceland, and also with the Faculty of Electronics, Telecommunications and Informatics, Gdansk University of Technology, 80-233 Gdansk, Poland (e-mail: Koziel@ru.is).

Iftikhar ud Din is with the Telecommunication Engineering Department, University of Engineering and Technology, Mardan 23200, Pakistan (e-mail: iftikharuddin114@gmail.com).

Bruno Cavalcante de Souza Sanches is with the Department of Electronic Systems Engineering, Escola Politécnica da Universidade de São Paulo, São Paulo 05508-900, Brazil (e-mail: bruno.csanches@usp.br).

REFERENCES

[1] C. Yu, S. Fan, Y. Sun, and E. Pickwell-MacPherson, "The potential of terahertz imaging for cancer diagnosis: A review of investigations to date," *Quant. Imag. Med. Surg.*, vol. 2, no. 1, p. 33, 2012.

[2] A. Lomas, J. Leonardi-Bee, and F. Bath-Hextall, "A systematic review of worldwide incidence of nonmelanoma skin cancer," *Brit. J. Dermatol.*, vol. 166, no. 5, pp. 1069–1080, May 2012.

[3] R. S. Stern, "Prevalence of a history of skin cancer in 2007: Results of an incidence-based model," *Arch. Dermatol.*, vol. 146, no. 3, pp. 279–282, 2010.

[4] V. Samarasinghe and V. Madan, "Nonmelanoma skin cancer," *J. Cutaneous Aesthetic Surg.*, vol. 5, no. 1, p. 3, 2012.

[5] B. T. Beal et al., "Patients' body image improves after Mohs micrographic surgery for nonmelanoma head and neck skin cancer," *Dermatolog. Surg.*, vol. 44, no. 11, pp. 1380–1388, 2018.

[6] A. Di Stefani and S. Chimenti, "Basal cell carcinoma: Clinical and pathological features," *Giornale Italiano Di Dermatologia E Venereologia, Organo Ufficiale, Societa Italiana Di Dermatologia E Sifilografia*, vol. 150, no. 4, pp. 385–391, 2015.

[7] A. Waldman and C. Schmults, "Cutaneous squamous cell carcinoma," *Hematol./Oncol. Clinics*, vol. 33, no. 1, pp. 1–12, 2019.

[8] M. N. Hamza and M. T. Islam, "Designing an extremely tiny dual-band biosensor based on MTMs in the terahertz region as a perfect absorber for non-melanoma skin cancer diagnostics," *IEEE Access*, vol. 11, pp. 136770–136781, 2023.

[9] B. Ghafari, M. Danaie, and M. Afsahi, "Perfect absorber based on epsilon-near-zero metamaterial as a refractive index sensor," *Sens. Imag.*, vol. 24, no. 1, p. 15, May 2023.

[10] D. Egemen et al., "Artificial intelligence–based image analysis in clinical testing: Lessons from cervical cancer screening," *J. Nat. Cancer Inst.*, vol. 116, no. 1, pp. 26–33, Jan. 2024.

[11] V. Faramarzi, M. Heidari, N. H. B. N. Zulkarnine, and M. T. Hwang, "Plasmonic biosensors based on deformed graphene," *Biophysica*, vol. 2, no. 4, pp. 538–547, Nov. 2022.

[12] M. Berka et al., "A miniaturized folded square split ring resonator cell based dual band polarization insensitive metamaterial absorber for C- and Ku-band applications," *Opt. Quantum Electron.*, vol. 55, no. 8, p. 699, Aug. 2023.

[13] G. Xuan, L. Gu, R. Peng, and H. Hu, "The optical chiral properties of double-layer T-shaped plasmonic array," *Plasmonics*, vol. 19, no. 1, pp. 159–165, Feb. 2024.

[14] M. Li, H.-L. Yang, X.-W. Hou, Y. Tian, and D.-Y. Hou, "Perfect metamaterial absorber with dual bands," *Prog. Electromagn. Res.*, vol. 108, pp. 37–49, 2010.

[15] N. Misran, S. H. Yusop, M. T. Islam, and M. Y. Ismail, "Analysis of parameterization substrate thickness and permittivity for concentric split ring square reflectarray element," *Jurnal Kejuruteraan, J. Eng.*, vol. 23, pp. 11–16, Nov. 2012.

[16] M. Z. Mahmud, M. T. Islam, N. Misran, S. Kibria, and M. Samsuzzaman, "Microwave imaging for breast tumor detection using uniplanar AMC based CPW-fed microstrip antenna," *IEEE Access*, vol. 6, pp. 44763–44775, 2018.

[17] A. Rahman, M. T. Islam, M. J. Singh, S. Kibria, and M. Akhtaruzzaman, "Electromagnetic performances analysis of an ultra-wideband and flexible material antenna in microwave breast imaging: To implement a wearable medical bra," *Sci. Rep.*, vol. 6, no. 1, p. 38906, Dec. 2016.

[18] S. Nourinovin, M. M. Rahman, M. Naftaly, M. P. Philpott, Q. H. Abbasi, and A. Alomainy, "Highly sensitive terahertz metasurface based on electromagnetically induced transparency-like resonance in detection of skin cancer cells," *IEEE Trans. Biomed. Eng.*, early access, Feb. 9, 2024, doi: 10.1109/TBME.2024.3364386.

[19] Z. Vafapour, E. S. Lari, and M. R. Forouzeshfard, "Breast cancer detection capability of a tunable perfect semiconductor absorber: Analytical and numerical evaluation," *Opt. Eng.*, vol. 60, no. 10, Oct. 2021, Art. no. 107101.

[20] Z. Vafapour, W. Troy, and A. Rashidi, "Colon cancer detection by designing and analytical evaluation of a water-based THz metamaterial perfect absorber," *IEEE Sensors J.*, vol. 21, no. 17, pp. 19307–19313, Sep. 2021.

[21] N. Rajaram, J. S. Reichenberg, M. R. Migden, T. H. Nguyen, and J. W. Tunnell, "Pilot clinical study for quantitative spectral diagnosis of non-melanoma skin cancer," *Lasers Surg. Med.*, vol. 42, no. 10, pp. 876–887, 2010.

[22] A. Hamouleh-Alipour, M. Forouzeshfard, R. Baghbani, and Z. Vafapour, "Blood hemoglobin concentration sensing by optical nano biosensor-based plasmonic metasurface: A feasibility study," *IEEE Trans. Nanotechnol.*, vol. 21, pp. 620–628, 2022.

[23] Z. Vafapour, "Cost-effective bull's eye aperture-style multi-band metamaterial absorber at sub-THz band: Design, numerical analysis, and physical interpretation," *Sensors*, vol. 22, no. 8, p. 2892, Apr. 2022.

[24] G. Sun, Y. Chen, Q. Wang, and D. Wang, "Polarization-and angle-insensitive broadband long wavelength infrared absorber based on coplanar four-sized resonators," *Opt. Exp.*, vol. 31, no. 16, pp. 26344–26354, 2023.

[25] M. Berka, B. Fellah, S. Das, T. Islam, S. Asha, and Z. Mahdjoub, "Nano-resonator based broadband metamaterial absorber with angular stability operating in visible light spectrum for solar energy harvesting applications," *Opt. Mater.*, vol. 149, Mar. 2024, Art. no. 115043.

[26] A. Banerjee, S. Vajandar, and T. Basu, "Prospects in medical applications of terahertz waves," in *Terahertz Biomedical and Healthcare Technologies*. Amsterdam, The Netherlands: Elsevier, 2020, pp. 225–239.

[27] I. V. A. K. Reddy, S. Elmaadawy, E. P. Furlani, and J. M. Jornet, "Photothermal effects of terahertz-band and optical electromagnetic radiation on human tissues," *Sci. Rep.*, vol. 13, no. 1, p. 14643, Sep. 2023.

[28] M. Gezimati and G. Singh, "Advances in terahertz technology for cancer detection applications," *Opt. Quantum Electron.*, vol. 55, no. 2, p. 151, Feb. 2023.

[29] P. W. Kolb, T. S. Salter, J. A. McGee, H. D. Drew, and W. J. Padilla, "Extreme subwavelength electric GHz metamaterials," *J. Appl. Phys.*, vol. 110, no. 5, Sep. 2011, Art. no. 054906.

[30] R. Contractor, G. D'Aguanno, and C. Menyuk, "Ultra-broadband, polarization-independent, wide-angle absorption in impedance-matched metamaterials with anti-reflective moth-eye surfaces," *Opt. Exp.*, vol. 26, no. 18, p. 24031, 2018.

[31] R. M. H. Bilal, M. A. Saeed, M. A. Naveed, M. Zubair, M. Q. Mehmood, and Y. Massoud, "Nickel-based high-bandwidth nanostructured metamaterial absorber for visible and infrared spectrum," *Nanomaterials*, vol. 12, no. 19, p. 3356, Sep. 2022.

[32] I. Tathfif, M. F. Hassan, K. S. Rashid, A. A. Yaseer, and R. H. Sagor, "A highly sensitive plasmonic refractive index sensor based on concentric triple ring resonator for cancer biomarker and chemical concentration detection," *Opt. Commun.*, vol. 519, Sep. 2022, Art. no. 128429.

[33] M. Danaie and B. Kiani, "Design of a label-free photonic crystal refractive index sensor for biomedical applications," *Photon. Nanostruct.-Fundam. Appl.*, vol. 31, pp. 89–98, Sep. 2018.

[34] A. Shrivastava, S. Saini, P. Kumar, and S. Singh, "A potential absorber for PHz electronics using Sn/h-BN van der Waals structure: A hybrid DFT and macroscopic investigations," *Phys. E, Low-Dimensional Syst. Nanostruct.*, vol. 144, Oct. 2022, Art. no. 115423.

[35] T. Suzuki, M. Sekiya, T. Sato, and Y. Takebayashi, "Negative refractive index metamaterial with high transmission, low reflection, and low loss in the terahertz waveband," *Opt. Exp.*, vol. 26, no. 7, pp. 8314–8324, Apr. 2018.

[36] M. M. K. Shuvo et al., "Polarization and angular insensitive bendable metamaterial absorber for UV to NIR range," *Sci. Rep.*, vol. 12, no. 1, p. 4857, Mar. 2022.

[37] H. Liu, K. Luo, S. Tang, D. Peng, F. Hu, and L. Tu, "An ultra-wideband THz/IR metamaterial absorber based on doped silicon," *Materials*, vol. 11, no. 12, p. 2590, Dec. 2018.

[38] F. Lou, J. Lei, K. Huan, and J. Lin, "Simple quad-band terahertz metamaterial absorber based on high-order plasmon resonance for sensing applications," *J. Nanophotonics*, vol. 16, no. 1, Feb. 2022, Art. no. 016010.

[39] L. Lei, S. Li, H. Huang, K. Tao, and P. Xu, "Ultra-broadband absorber from visible to near-infrared using plasmonic metamaterial," *Opt. Exp.*, vol. 26, no. 5, p. 5686, 2018.

[40] R. Lai, P. Shi, Z. Yi, H. Li, and Y. Yi, "Triple-band surface plasmon resonance metamaterial absorber based on open-ended prohibited sign type monolayer graphene," *Micromachines*, vol. 14, no. 5, p. 953, Apr. 2023.

[41] M. L. Hakim et al., "Ultrawideband polarization-independent nanoarchitectonics: A perfect metamaterial absorber for visible and infrared optical window applications," *Nanomaterials*, vol. 12, no. 16, p. 2849, Aug. 2022.

[42] S. Patel, S. K. Patel, A. H. M. Almawgani, A. Armghan, A. Alzahrani, and S. A. Taya, "Numerical study of graphene-based wideband solar absorber using MIM structure for solar thermal energy conversion," *Adv. Theory Simulations*, vol. 7, no. 1, Jan. 2024, Art. no. 2300352.

[43] S. Mahmud, S. S. Islam, K. Mat, M. E. H. Chowdhury, H. Rmili, and M. T. Islam, "Design and parametric analysis of a wide-angle polarization-insensitive metamaterial absorber with a star shape resonator for optical wavelength applications," *Results Phys.*, vol. 18, Sep. 2020, Art. no. 103259.

[44] I. H. Chowdhury, M. M. R. Mazumder, S. S. Islam, M. T. Islam, M. S. Soliman, and M. S. Islam, "Ultrawideband nanostructured metamaterial absorber with an octagon-packed star-shaped resonator for UV to NIR spectrum wavelength application," *Ain Shams Eng. J.*, vol. 15, no. 4, Apr. 2024, Art. no. 102653.

[45] A. Musa et al., "Broadband plasmonic metamaterial optical absorber for the visible to near-infrared region," *Nanomaterials*, vol. 13, no. 4, p. 626, Feb. 2023.

[46] S. Jiao, Y. Li, H. Yang, and S. Xu, "Numerical study of ultra-broadband wide-angle absorber," *Results Phys.*, vol. 24, May 2021, Art. no. 104146.

[47] R. M. H. Bilal, S. Zakir, M. A. Naveed, M. Zubair, M. Q. Mehmood, and Y. Massoud, "Nanoengineered nickel-based ultrathin metamaterial absorber for the visible and short-infrared spectrum," *Opt. Mater. Exp.*, vol. 13, no. 1, pp. 28–40, 2023.

[48] D. Wu, L. Lei, M. Xie, P. Xu, and S. Xu, "High-performance metamaterial light absorption from visible to near-infrared assisted by anti-reflection coating," *Photonics*, vol. 10, no. 9, p. 998, Aug. 2023.

[49] M. S. Raeen, A. Nella, and R. Maheswar, "A fourfold star petal–shaped polarization-insensitive broadband plasmonic metamaterial absorber," *Plasmonics*, vol. 18, no. 3, pp. 1059–1074, Jun. 2023.

[50] F. Yang, R.-H. Li, S.-L. Tan, J.-W. Dong, and S.-J. Jiang, "Visible-mid infrared ultra-broadband and wide-angle metamaterial perfect absorber based on cermet films with nano-cone structure," *Nanophotonics*, vol. 12, no. 13, pp. 2451–2460, Jun. 2023.

[51] A. Hanif et al., "Ni-PI-Ni based nanoarchitectonics near-perfect metamaterial absorber with incident angle stability for visible and near-infrared applications," *Int. J. Optomechatronics*, vol. 18, no. 1, Dec. 2024, Art. no. 2299026.

[52] K. Ahmed, B. K. Paul, F. Ahmed, M. A. Jabin, and M. S. Uddin, "Numerical demonstration of triangular shaped photonic crystal fibre-based biosensor in the terahertz range," *IET Optoelectronics*, vol. 15, no. 1, pp. 1–7, Feb. 2021.

[53] M. A. Jabin et al., "Surface plasmon resonance based titanium coated biosensor for cancer cell detection," *IEEE Photon. J.*, vol. 11, no. 4, pp. 1–10, Aug. 2019.
[54] P. Kumar, V. Kumar, and J. S. Roy, "Dodecagonal photonic crystal fibers with negative dispersion and low confinement loss," *Optik*, vol. 144, pp. 363–369, Sep. 2017.
[55] T. Parvin, K. Ahmed, A. M. Alatwi, and A. N. Z. Rashed, "Differential optical absorption spectroscopy-based refractive index sensor for cancer cell detection," *Opt. Rev.*, vol. 28, no. 1, pp. 134–143, Feb. 2021.
[56] P. Sharma, P. Sharan, and P. Deshmukh, "A photonic crystal sensor for analysis and detection of cancer cells," in *Proc. Int. Conf. Pervasive Comput. (ICPC)*, Jan. 2015, pp. 1–5.
[57] S. J. Park et al., "Detection of microorganisms using terahertz metamaterials," *Sci. Rep.*, vol. 4, no. 1, p. 4988, May 2014.
[58] S. J. Park, S. H. Cha, G. A. Shin, and Y. H. Ahn, "Sensing viruses using terahertz nano-gap metamaterials," *Biomed. Opt. Exp.*, vol. 8, no. 8, pp. 3551–3558, 2017.
[59] T. Chen, D. Zhang, F. Huang, Z. Li, and F. Hu, "Design of a terahertz metamaterial sensor based on split ring resonator nested square ring resonator," *Mater. Res. Exp.*, vol. 7, no. 9, Sep. 2020, Art. no. 095802.
[60] S. Asgari, N. Granpayeh, and T. Fabritius, "Controllable terahertz cross-shaped three-dimensional graphene intrinsically chiral metastructure and its biosensing application," *Opt. Commun.*, vol. 474, Nov. 2020, Art. no. 126080.
[61] J. Yang and Y.-S. Lin, "Design of tunable terahertz metamaterial sensor with single- and dual-resonance characteristic," *Nanomaterials*, vol. 11, no. 9, p. 2212, Aug. 2021.
[62] C. Tan et al., "Cancer diagnosis using terahertz-graphene-metasurface-based biosensor with dual-resonance response," *Nanomaterials*, vol. 12, no. 21, p. 3889, Nov. 2022.
[63] H. Hu, B. Qi, Y. Zhao, X. Zhang, Y. Wang, and X. Huang, "A graphene-based THz metasurface sensor with air-spaced structure," *Frontiers Phys.*, vol. 10, Sep. 2022, Art. no. 990126.
[64] E. Hoseini, A. Mir, and A. Farmani, "Modeling and proposal of a black phosphorus-based nanostructure for detection of avian influenza virus in infrared region," *Opt. Quantum Electron.*, vol. 54, no. 10, p. 609, Oct. 2022.

Musa N. Hamza received the B.Sc. degree from the Department of Physics, Faculty of Science and Health, Koya University, Koy Sanjaq, Iraq, in 2015, and the M.Sc. degree from the Department of Medical Physics, College of Medical and Applied Sciences, Charmo University, Chamchamal, Sulaymaniyah, in 2023.

His research interests include medical physics, the diagnosis of different types of cancer at an early stage, antenna arrays, metamaterials, sensors, and biosensors.

Mohammad Tariqul Islam (Senior Member, IEEE) is currently a Professor with the Department of Electrical, Electronic and Systems Engineering, Universiti Kebangsaan Malaysia (UKM), Bangi, Malaysia, and a Visiting Professor with the Kyushu Institute of Technology, Kitakyushu, Japan. He is the author and coauthor of about 600 research journal articles, nearly 250 conference articles, and a few book chapters on various topics related to antennas, metamaterials, and microwave imaging with 25 inventory patents filed. Thus far, his publications have been cited 15 700 times and his H-index is 56 (Source: Scopus). His Google Scholar citation is 25 000 and H-index is 66. His research interests include communication antenna design, metamaterial, satellite antennas, and microwave imaging.

Dr. Islam is a Fellow of IET, U.K., and a Senior Member of IEICE, Japan. He was a recipient of more than 40 research grants from Malaysian Ministry of Science, Technology and Innovation, Ministry of Education, UKM research grant, and international research grants from Japan, Saudi Arabia, and Kuwait. He served as an Executive Committee Member for IEEE AP/MTT/EMC Malaysia Chapter, from 2019 to 2020 and a Chartered Professional Engineer (CEng). He received several International Gold Medal awards, the Best Invention in Telecommunication Award for his research and innovation, and the Best Researcher Award at UKM. He was a recipient of the 2018, 2019, and 2020 IEEE AP/MTT/EMC Malaysia Chapter, Excellent Award. He also won the best innovation award and the Best Researcher award by UKM, in different years. He was a recipient of the Publication Award from the Malaysian Space Agency for several years. He has supervised about 50 Ph.D. theses and 30 M.Sc. theses, and has mentored more than ten postdocs and visiting scholars. He has developed the Antenna Measurement Laboratory which includes antenna design and measurement facility till 40 GHz. He was an Associate Editor of *IET Electronics Letter*. He also serves as the Guest Editor of the *Sensors* journal and *Nanomaterials* and an Associate Editor for IEEE ACCESS.

Sunil Lavadiya (Member, IEEE) received the B.Tech. degree in electronics and communication from Saurashtra University, Rajkot, India, in 2008, the M.Tech. degree in communication engineering from Nirma University, Ahmedabad, India, in 2010, and the Ph.D. degree in high gain frequency reconfigurable liquid metamaterial microstrip patch antenna from Marwadi University, Rajkot, Gujarat, India, in 2022.

He working as an Associate Professor at the Department of Information and Communication Technology, Marwadi University, Rajkot. He has adapted to all aspects of Electronics and Communication Engineering, including training, education, and research. He works in the MIMO, sensors, reconfigurable, superstrate, solar absorber, and liquid antennas. He has published 50 SCI research articles, 12 Scopus index articles, eight book chapters, and five papers in an international conference and filed four design patents and one copyright.

Dr. Lavadiya is a member of IETE.

Slawomir Koziel (Fellow, IEEE) received the M.Sc. and Ph.D. degrees in electronic engineering from Gdansk University of Technology, Gdansk, Poland, in 1995 and 2000, respectively, the M.Sc. degree in theoretical physics, and the M.Sc. degree in mathematics, and the Ph.D. degree in mathematics from the University of Gdansk, Gdansk, in 2000, 2002, and 2003, respectively.

He is currently a Professor with the Department of Engineering, Reykjavik University, Reykjavik, Iceland. His research interests include CAD and modeling of microwave and antenna structures, simulation-driven design, surrogate-based optimization, space mapping, circuit theory, analog signal processing, evolutionary computation, and numerical analysis.

Iftikhar ud Din received the B.Sc. and M.Sc. degrees in telecommunication engineering from the University of Engineering and Technology, Peshawar, Pakistan, in 2017 and 2021 respectively.

His current research interests include UWB antennas, FSS-based UWB antennas, and sub-6 GHz 5G antennas, 5G millimeter wave antennas and MIMO antennas, frequency selective surfaces, EBGs, and metamaterial-based antenna.

Dr. ud Din is a member of the Antennas and Microwave Engineering Research Group (AMERG), University of Engineering & Technology (UET), Mardan, Pakistan.

Bruno Cavalcante de Souza Sanches (Member, IEEE) received the bachelor's degree in information engineering and the master's degree in energy from the Federal University of ABC, Santo André, Brazil, in 2011 and 2013, respectively, and the Ph.D. degree in microelectronics from the Integrated Systems Laboratory (LSI), University of São Paulo, São Paulo, Brazil, in 2021.

In 2017, he began working as an Engineering Professor. He is working on the design of a novel mixed-signal integrated circuit used in the ALICE experiment in the CERN LHC. He has more than 15 years of experience in electronics and microelectronics design. He has been involved in hardware development, smart grids, algorithms, artificial intelligence, digital communication systems, EDA tools, electronics for high-energy physics experiments, and several systems targeting early cancer detection including bioimpedance spectroscopy and microwave imaging.